eprints@whiterose.ac.uk
https://eprints.whiterose.ac.uk/

Towards a microbubble condenser: Dispersed microbubble mediation of additional heat transfer in aqueous solutions due to phase change dynamics in airlift vessels

William B. Zimmerman

Department of Chemical and Biological Engineering, University of Sheffield, Mappin Street, Sheffield S1 3JD, United Kingdom

HIGHLIGHTS

- New theory for heat transfer via microbubble mediated solvent phase change.
- Prediction for heat transfer coefficient/microbubble phase fraction correlation.
- Consistent with analysis of freezing onset for boiled water placed in a freezer.
- Inferred HTCs are inversely correlated related to oxygen solubility at onset temp.
- Supports assertion that microbubble phase fraction is controlled by initial temp.

ARTICLE INFO

ABSTRACT

Microbubbles dispersions in aqueous solutions can be long lived. For instance, 20micron size microbubbles take on the order of a day to rise one meter. Consequently, any currents in a reasonably sized vessel would be expected to entrain such a microbubble dispersion as the buoyant force is exceeded by the inertial force of liquid currents. This paper argues for the advantages of a microbubble dispersion mediated condenser with two benefits. The obvious advantage over fine bubble direct contact heating or cooling is that the microbubble phase, which can be engineered with a throughput of approximately a hectare per second of interfacial area flux per cubic meter of solution volume, should not be limited by heat transfer to and from the liquid and microbubble phase. Rather the limitation will be on the wetted area for heat transfer of the vessel to its heat exchange configuration. The second potential advantage follows from the theory proposed in this paper. Arranging the condenser in the microbubble mediated airlift configuration will introduce additional heat transfer from microbubbles vaporizing hotter water near the central plume and convecting that additional latent heat to the cold wall, which condenses the water vapor and releases the latent heat. This additional convection of latent heat is proposed as an additional source term for heat transport equation, and the magnitude of the effect is shown to be proportional to the phase fraction of microbubbles. This theory is shown to be consistent with analysis of observations of freezing times measured by Mpemba and Osborne [Phys. Educ. 4:172-5, 1969], that infer heat transfer coefficients from fitting Newton's law of cooling. The inferred heat transfer coefficient ratio from the presumed highest microbubble phase fraction to the lowest is ~7.4:1. Whether or not that enhancement level persists to a microbubble condenser in an airlift vessel, the promise of additional heat transfer should be explored.
© 2021 The Author. Published by Elsevier Ltd. This is an open access article under the CC BY license (http://creativecommons.org/licenses/by/4.0/).

1. Introduction

Zalba et al. (2003) review phase change as a methodology for heat storage. Generally, we think of heat storage in terms of the heat capacity of a material. But heat applied to achieve phase change can be stored potentially more densely than in a single phase material. For instance, the latent heat of vaporization of water held by a vapour is potentially equivalent to the excess enthalpy of heating a liquid to a very high temperature. Yet, sensible heat transfer from the vessel can recoup the stored heat when needed. Conversely, the cooling potential occurs by evaporation into relatively dry, sub-saturated gas. The cooling potential of perspiration, for instance, lies in the drawing of the latent heat of vaporization from the material in contact with the liquid being evaporated. Commercial heat storage systems, such as that of

Nomenclature

c_p	Heat capacity at constant pressure [J/kgK]		T	Temperature [K]
c^*	Saturation concentration [mol/m^3]		t	Time coordinate [s]
F	Latent heat density within dispersed microbubbles [J/m^3]		v	Velocity [m/s]
			α	Thermal diffusivity Special characters
h	Bubble heat transfer coefficient [W m^{-2} K^{-1}]		ϕ	Microbubble phase fraction [m^2/s]
N_{Mpemba}	Dimensionless function of temperature [-]		κ	Thermal conductivity [-]
p	Pressure scalar [N/m^2]		ρ	Density [W/mK]
P^*	Saturation pressure [N/m^2]		ξ	Exponential decay rate proportional the HTC [kg/m^3]
$q,$	Heat flux [W/m^2]		ξ	[s^{-1}]
Q_{xs}	Estimate of additional heat transfer [kJ m^{-3}]			
R	Gas constant [J/molK]			
s^*	Total gas solubility (oxygen exemplar) [mg L^{-1}]			

Steffes (Wies and Jannsen, 2014) are limited to water, or in general to cheap heat transfer materials, due to the high cost of high performance heat storage materials. The potential for dispersal of microbubbles that would increase the heat storage capacity via phase change is worth exploring, particularly if microbubble dispersions enhanced the heat transfer performance for both transfer in and out of heat in normal operations.

Dispersal of materials in composites, both liquid and solid, have long been known to dramatically change transfer properties. For instance, Shaqfeh (1988) derived a theory for transport properties of composite materials that naturally leads to a nonlocal description of effective properties. Anisotropy (more rapid transfer in one direction than another) is one outcome that can be engineered by dispersal of one phase in another. You and Kim (2003) have shown that a nanofluid comprising of water mixed with extremely small amount of dispersed nanosized particles achieves 200% greater heat transfer than water alone. Lervik et al. (2009) estimated the enhancement in interfacial conductance for a nanofluid suspension consisting of dispersed nanodroplets, showing an increase in the thermal conductivity with decreasing nanodroplet radius, consistent with experimental studies of nanofluids. What is missing from these samples of enhancement of heat transfer is dispersed micro/nanobubbles.

The paper is organized as follows. A theory for the role of micro/nanobubbles in accelerating heat transfer is presented that illustrates the components of the mechanism for convective temperature cycling of micro/nanobubbles providing additional heat transport. The theory is tested by *de novo* analysis of datasets of Mpemba and Osborne (1969) where the argument is made that microbubbles are introduced with substantially different phase fractions across the range of experiments. Excellent agreement is found from correlating the heat transfer coefficients inferred with the proposed mechanism for microbubble phase fraction variation, providing strong support for the new theory. The theory section includes the motivation for how microbubble condensers, a conceptual advance on the existing class of direct contact fine bubble heating/cooling unit operations, would benefit from the additional heat transfer hypothesized from dispersal of microbubbles, as well as an explanation for why fine bubbles do not provide such intensification. The theory section develops estimates of the scale of the additional heat transfer mechanism and derives a transport equation from control volume analysis with the additional phase change convective term for carrying latent heat. A dimensionless number for the additional heat flux induced by dispersed microbubbles is proposed, and shown to be proportional to the microbubble phase fraction. It is this functionality that is correlated with heat transfer coefficient estimates of Mpemba and Osborne in the Discussion and Analysis section. The paper finishes

with a conclusion section that quantifies the correlation and summarises the conclusions drawn.

2. Theory of microbubble mediated heat transfer dynamics

2.1. Motivation

Instructors of creativity courses tell us that necessity is not the mother of invention. For instance microbubble distillation (described in Fig. 1, describing Zimmerman et al. (2013)) was not invented due to a crisis in distillation technology. Rather, the parents of invention are observation and curiosity – particularly the curiosity of finding a viewpoint for how the world might be different or engineered to be different from how it is currently perceived. The invention of microbubble distillation (Zimmerman et al. 2013) had a codicil observation. The major invention occurs by restricting the contact time of an injected microbubble of size ~ 200 μm in diameter to the period of time just surrounding the maximum in absolute humidity. This is done by limiting the liquid layer height and/or increasing the injection velocity of the microbubble, i.e. approximately 1 ms from the right panel for Fig. 1. This restriction then achieves the maximum rate of evaporation. It turns out that because this period corresponds to high non-equilibrium thermochemical driving force, you also achieve maximum separation of volatile liquid mixtures. Abdulrazzaq et al. (2016) and Al-yaqoobi (2016) showed that it could achieve highly enriched partition coefficients for ethanol in ethanol–water separations. Abdulrazzaq et al. (2015) demonstrated an effective strategy to use microbubble distillation to break binary liquid azeotropes. Desai (2017) estimated in ammonia-water separations that hot microbubble distillation achieves 1000–3000 fold the mass transfer coefficient of fine bubble diffusers commonly used in wastewater aeration.

The codicil observation, clear from the right panel of Fig. 1, is that after the maximum absolute humidity is achieved, if the contacting is permitted to continue (higher liquid layer height), then the configuration acts as a microbubble condenser, eventually achieving thermochemical equilibrium. Not quite clear, however is that microbubbles of the order of 200 μm in diameter achieve thermochemical equilibrium in ~ 3 ms of contact time, i.e. a few centimeters at terminal velocity. Conversely, because coarse bubbles rise 3 orders of magnitude faster than said microbubbles, it takes tens of meters of liquid column height to achieve thermochemical equilibrium. Microbubble distillation engineers within that millisecond timescale to exploit non-equilibrium chemical thermodynamic drivers. Microbubble condensation, however, has the feature that for not much longer length scale, i.e. conventional scale vessels down to common food containers, like ice cream containers, thermochemical equilibrium is rapidly established.
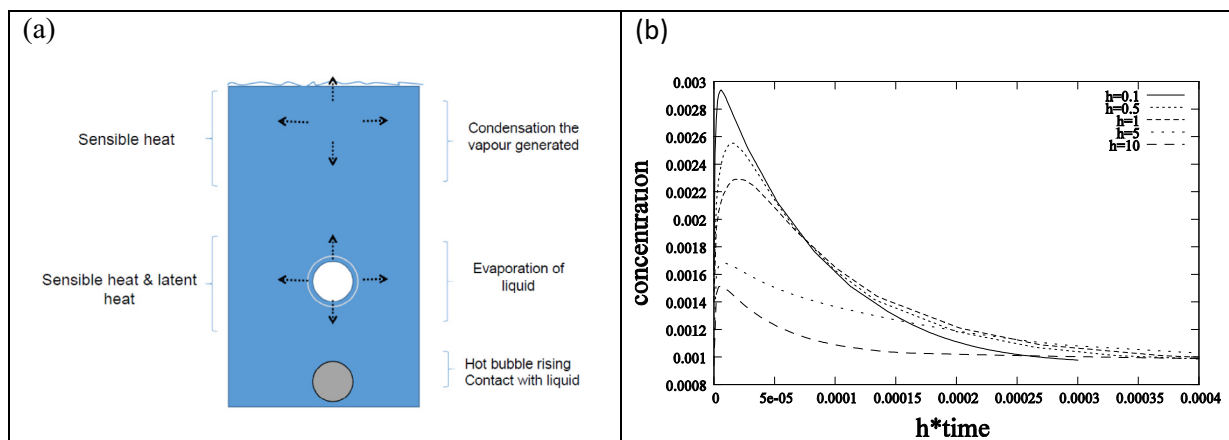
Fig. 1. The principles underpinning microbubble distillation and condensation. (a) If a hot, dry microbubble of air is injected into water, it has two mechanisms available to it – sensible heat transfer to the hot liquid and evaporation which expends the latent heat of vaporisation. It turns out that for microbubbles introduced into laminar flow, evaporation occurs very rapidly, but sensible heat transfer is slow, due to the laminar boundary layer providing resistance to heat transfer. Subsequently, if the microbubble continues to rise, it passes through a maximum absolute humidity (b), whereupon the dominant effect is condensation of the already vaporized water vapour as the bubble continuous to cool. The levels of h (bubble heat transfer coefficients in W m^{-2} K^{-1}) are proxy for the bubble diameter, where $h = 10$ is equivalent to a coarse bubble of diameter ∼ 1 cm, and $h = 0.1$ to a microbubble of diameter ∼ 200microns. Adapted from Zimmerman et al. (2013). Note concentration has units of mol m^{-3}; time is in seconds.

Direct contact coolers / condensers are not new. Francis and Pashley (2009) have exploited this feature for a fine bubble evaporation-based desalination process. MIT's spinout company Gradiant exploits direct contact fine bubble condenser to purify fracking produced wastewater (Matheson, 2015). The configuration schematically for a fine bubble condenser is shown in Fig. 2 (a). It is clear that the limitation for cooling efficiency is either the residence time of the bubble, according to Fig. 1(b) or the exterior heat transfer surface area of the condenser vessel. So the substitution of microbubbles in place of fine bubbles has the promise of removing the bottleneck of hot bubble to cold water heat transfer, as the two phases will thermally and chemically equilibrate within a few centimetres of rising in the cold water. The MIT process is slightly more complicated as the injected water vapour-rich gas is the offgas from stripping water vapour from an evaporator with fracking produced water as the substrate. It will contain hydrocarbon and acid gases as well as the water vapour. In this sense, the Gradiant fine bubble condenser preferentially serves as a *partial* condenser – letting the lower boiling point and permanent gases pass through while condensing high purity water.
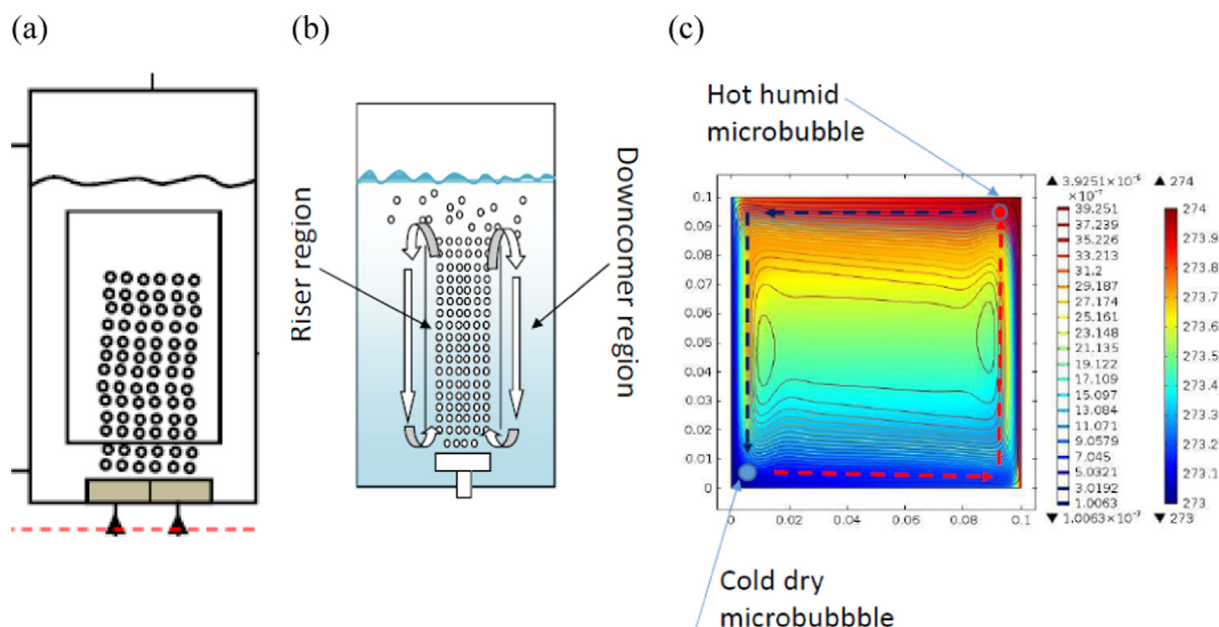
Fig. 2. So what advantage does a microbubble condenser have over a conventional direct contact cooler? (a) a direct contact cooler has fairly unidirectional flow with large bubbles rising vertically, dragging very little liquid with them, and short contact time. (b) A microbubble condenser naturally adopts an airlift loop configuration where bubbles rise in the centre but the sub-100 μm microbubbles are entrained and recirculate according to Al-Mashhadani et al (2015). This circulatory flow of the microbubbles can be interpreted as ducting microbubbles through the hot region in the center (similar to rising along a hot wall in the canonical hot-wall cold wall problem) and then falling along the cold wall of the downcomer region. (c) The arrows show how the absolute humidity of the bubble cycles during this a free convection flow. Color represents temperature (K) according to the variation shown from 274 K (hot right wall) to 273 K (cold left wall). The streamlines are level sets of the streamfunction, which is non-dimensionalized relative to the velocity scale as reported in Zimmerman (2006). 'Cold dry microbubble' labels the position where the absolute humidity and temperature of the microbubble is minimal. 'Hot humid microbubble' labels the position of maximum absolute humidity and temperature. The inference from Zimmerman et al. (2013) is that all microbubbles are nearly saturated (100% humidity) due to the millisecond response time.

Since direct contact fine bubble condensers are not new, what is the potential benefit of microbubbles? Given the short contact time to equilibration, also thought of as a quick thermochemical response time of microbubbles, the microbubble condenser will not be limited by bubble-water heat or mass transfer. Conceptually, for a cubic metre of condenser vessel, with the throughput of gas of the TataSteel microalgae pilot scale trials for scrubbing CO_2-rich stack gas to provide the C-source for the bioculture (Zimmerman et al. 2011a), and the microbubble average size achievable in recent tuning studies aimed at dispersed air flotation (Desai et al., 2018), approximately a hectare per second microbubble flux is possible. Such a process would rapidly reach a pseudo-steady state that is limited in heat flux by the wetted surface area of the condenser vessel. For instance, the exterior walls of Fig. 2b are the limitation on heat exchange in general, but in an airlift loop configuration, the interior baffle can be replaced by a coiled internal heat exchanger as popularized by Nigam and coworkers (see, e.g. Kumar et al., 2008). Thus, in order for microbubbles to be a major advance upon fine bubble direct contact condensers, they should ideally mitigate this limitation.

The speculation underpinning this paper is that the airlift loop configuration for a microbubble bioreactor, studied by Al-Mashhadani et al. (2015) is the proper class of design for a microbubble direct contact condenser, as shown schematically in Fig. 2 (center frame). The insertion of the concentric baffle, presuming the bioreactor as shown is axisymmetric, helps to direct turbulent plumes. In laminar flow of microbubbles, it is almost superfluous as, without turbulent spreading of the plume, microbubble clouds of nearly monodisperse, uniformly spaced bubbles generated by fluidic oscillation, self-stabilize to rise in vertical "chains" (Zimmerman et al 2009). Al-Mashhadani et al. (2015) demonstrated two remarkable features of sub 100 μm size microbubbles driving this toroidal convection cell:

(i) liquid mixing is 10-fold faster in the riser and downcomer than when injected with fine bubbles;
(ii) a substantial fraction of sub 100 μm size bubbles are entrained in the downcomer region, and therefore form a procession around the toroidal convection cell.

As the walls of the Tata Steel microbubble ALB pilot plant were transparent, the procession of microalgae attached to microbubbles as an ephemeral floc could be observed, supporting the conclusions of microbubble procession / entrainment. Larger microbubbles are too buoyant to be entrained, so eventually burst at the upper gas–liquid surface.

Certainly the faster free convective motion will increase transverse mixing due to the toroidal flow structure, which automatically increases heat transfer by convection to the walls of the condenser vessel. Rapid removal of chilled fluid from the cool surface and renewal with warmer fluid inherently increases heat transfer rates. The well known hot wall-cold wall heat transfer problem for water was simulated by Zimmerman (2006) (Fig. 2, right frame), taking into account the non-monotonic density-temperature profile for water, which has a maximum density at 4 °C. It is well known that the Nusselt number (dimensionless heat transfer coefficient) is constructed as strongly dependent on the turnover rate of the convection cell.

The observation that microbubbles are entrained in the downcomer region of an ALB can be analysed, however, in the context of a hypothetical microbubble that traces the streamlines (contours in Fig. 2, right frame) during its motion. At the lower left – the bottom of the cold wall, a microbubble of air that is inserted would rapidly equilibrate thermally so its absolute humidity would be computed by its saturation pressure scaled by the abso-

lute temperature and the ideal gas constant: $c^*(T) = \frac{p^*(T)}{RT}$. As the microbubble is dragged by the convective liquid flow across the bottom of the vessel, it is continuously heated (color plot shows blue for cold, red for hot), but then is dramatically heated as it rises to the top of the liquid layer along the hot wall. When this microbubble reaches the top of column of liquid, it will have rapidly equilibrated in temperature, to its highest temperature and thus highest absolute humidity. It crosses along near the top surface and then cools rapidly as it drops along the cold wall, achieving again its coolest temperature and lowest absolute humidity. During this cycle, in addition to convecting sensible heat by the change of temperatures, the vaporization along the hot wall of water removed the latent heat of vaporization from the fluid near the hot wall, which creates an additional local temperature gradient that drives heat transfer to the liquid from the hot wall. Similarly, as the microbubble falls along the cold wall, it condenses water vapour that then releases the latent heat of vaporization, creating an additional local temperature gradient that is the "sinked" by the cold wall. In effect, the convection process carries latent heat from the hot wall to the cold wall, along with convecting sensible heat.

3. Analyzing the excess heat transfer mediated by vaporization-condensation cycling by microbubbles

The additional feature of the humidity variation during the procession of the microbubble along the streamline can be considered as an additional, distributed heat source or heat sink when the bubble enters the opposing thermal region. So, consider the hot bubble arriving at top right in Fig. 2 (right frame). As it moves from top right to top left, the bubble moves through a rapidly decreasing thermal gradient. Sensible heat transfer from the bubble draws the latent heat of vaporization from the gas and condenses some of the water. As the microbubble passes along the path from the top of the cold wall to the bottom, it relinquishes all its excess enthalpy from stored latent heat. The effect of the passage of a significant volume fraction of microbubbles along the cold wall is that this packet of fluid, and all along its, trajectory is hotter than it would have been without the bubble delivering its stored payload. Now consider Newton's law of cooling between this path of the fluid element and the cold wall:

$$q_{cw} = -h(T_{BC} - T_{cw}) \tag{1}$$

If T_{BC} (streamline temperature) is greater than it would otherwise have been in the absence of the additional bubble phase, then the resultant heat flux through the cold wall (q_{cw}) will be larger, assuming the same heat transfer coefficient due to the same convection profile. Hence the rate of cooling increases.

It is not necessary to make the assumption that heat storage is greater than the heat capacity that the equivalent volume of liquid would have carried, as the vessel is not necessarily completely filled, hence there is no restriction on the liquid volume. If the volume is completely liquid filled, then the effect of replacing liquid phase with bubbles, expressed through the bubble phase volume fraction ϕ, should be considered in the context of all mechanisms of thermal transport for the complex fluid mixture:

$$\frac{DT}{Dt} = \alpha \nabla^2 T \text{ where } \alpha = \frac{k}{\rho c_p}$$
$$\sim \frac{k_l(1-\phi) + k_g\phi}{\left[\rho_l(1-\phi) + \rho_g\phi\right]\left[c_{pl}(1-\phi) + c_{pg}\phi\right]} \sim \frac{k_l}{\rho_l c_{pl}(1-\phi)} \tag{2}$$

where the material derivative (transport in the Lagrangian frame) on the right is controlled by the thermal diffusivity α, which is defined through the heat conductivity k, density ρ and heat capacity

c_pThe subscripts on these quantities both refer to the liquid (l) and gas (g) phases, respectively, and the common mixing rule as a first approximation to dilute mixtures is used. Because the magnitude of the gas phase constants k_l, ρ_1, c_{pl}, is so much larger than their gas phase counterparts, neglecting the gas phase constants relative to the much larger terms in (2) is reasonable, so that the effect of the dilute microbubble phase on the thermal diffusivity is a fractional *increase*.

Although its magnitude depends on the volume of the bubble phase, the additional heat flux by bubble phase change storage can be estimated by the cycling of the bubble temperature. For instance taking the upper temperature to be 35 °C results in

$$Q_{xs} = -c^*(35°C)\Delta H_v(35°C) + c^*(0°C)\Delta H_v(0°C) \sim -80 kJ/m^3 \quad (3)$$

per cycle. The symbols in equation (3) and associated are defined in subsequent paragraphs, with the point of the estimate here just to assert that the possible level of phase change heat transfer could dwarf the common mechanisms of conduction and convection. To turn this into a power for heat rate removal, the circulation rate of the convective roll must be known, where c*(T) is the saturation molar concentration, taken from Zimmerman et al. (2013), computed from the Antoine equation for saturated vapour pressure of water. This excess heatingQ_{xs}heating estimate is per cubic meter of microbubble phase, which is distinctly smaller than the volume taken up by the bulk fluid comprising the water and the dispersed microbubble phase. $Q_{xs}$is also a "per cycle" estimate, so it is the maximum amount of additional heat transferred via vaporisation near the hot wall and condensation near the cold wall. The estimate of equation (3) is consistent with all the vaporization happening at once, and all the condensation happening at once, but the microbubble internal temperature modifies according to a differential process as it is convected. The latent heat of evaporation for T in Kelvin, with units of $\frac{kg\, m^2}{mol\, s^2}$, is found from this quartic polynomial fit of the tabulated data from the NIST database:

$$\Delta H_v(T) = 56462.6 - 43.1784T + 0.000962433T^2 + 0.0000035155T^3 - 8.9825 \times 10^{-10}T^4$$

To estimate the magnitude of the additional heat flux due to microbubble humidity cycling, the additional enthalpy convected by the bubble cloud must be analysed. The additional enthalpy of a bubble phase can be described by an auxiliary scalar function related to Q_{xs} defined as:

$$F(T) = c^*(T)\Delta H_V(T) = \frac{p^*(T)}{RT}\Delta H_V(T);$$
$$Q_{xs}(T_0, T_1) = F(T_1) - F(T_0) \quad (4)$$

where p* is the saturation pressure of water vapour at bubble temperature T. A differential control volume analysis for the heat transport yields an extra term to (2) from this convected quantity, where v is the free convection velocity field and vector calculus identities are used:

$$\rho c_p \frac{DT}{Dt} = k\nabla^2 T - \phi\nabla \cdot (vF) = k\nabla^2 T - \phi F\nabla \cdot v - \phi v \cdot (F'\nabla T) \quad (5)$$

on the assumptions that the phase fraction is uniformly distributed in space, the temperature of the dispersed bubble phase is in local equilibrium with the liquid temperature, and that the humidity state of the bubble phase adapts instantaneously to the bubble temperature by vaporization or condensation, thereby absorbing or releasing the latent heat of vaporization. The latter is a reasonable assumption given the support of the FEM simulations of Zimmerman et al. (2013) that microbubbles internally mix rapidly and equilibrate in humidity at the bubble temperature in a timescale of 10^{-3}s. The former is a gross approximation, as the heat transfer coefficient suggests that sensible heat transfer is much slower than vaporization, and requires a liquid layer of a few centimeters for sensible heat transfer to "catch up" with vaporization when microbubbles are injected at close to their terminal rise velocity (Zimmerman et al., 2013).

The Boussinesq assumption that free convection velocity fields are nearly divergence-free can be employed to neglect one of the additional terms on the RHS of (5), which leaves the other term as "standard" convection term with a temperature dependent coefficient, $(\phi F')$. This is a localized source or sink for the heat transport equation, but effectively it "re-scales" the conventional buoyant convection term, $\rho c_p v \cdot \nabla T$, implicit on the LHS of (5). Since this conventional term is responsible for the additional heat flux of buoyant convection over thermal diffusion, the additional heat transfer by the additional source term can be estimated grossly by the order of magnitude increase of this term in a ratio to the buoyant convection term:

$$N_{Mpemba} = \frac{\phi F'(T)}{\rho c_p} \quad (6)$$

where the ratio is a dimensionless number, proportional to the bubble phase fraction. Fig. 3 shows the calculation of the dimensionless function over the range of liquid water temperatures at atmospheric pressure, demonstrating that at high temperatures, the effect is magnified, whereas a low temperatures, it becomes much smaller than convectional buoyant convection for all phase fractions. The T = 373 K estimate suggest that for a phase fraction that might go unnoticed, ϕ = 1%, a $\sim$ 10% increase in the heat transfer (Nusselt number) over the case with no microbubbles present is estimated. It is asserted that this is a lower bound because the instantaneous release of the excess enthalpy would largely occur along the top of the cold wall in Fig. 2, but the slower microbubble heat transfer coefficient would delay the release all along the cold wall. Similarly the heating would occur all along the hot wall. Hence the heat transfer would be expected to be more effective by the expected delay mechanism. Testing this hypothesis is beyond the scope of this order of magnitude dimensional analysis and would require a finite element study more complicated than Zimmerman and Rees (2007) for a somewhat more detailed mathematical model.

4. Discussion and analysis

Ideally, the theory presented here for augmented heat transfer due to microbubble mediated phase change in a free convection flow should be tested with a customized experiment to test the major prediction – the additional heat flux due to the presence of a dispersed microbubble phase that has a bubble size distribution less than, say, 100 μm. Such a constructive experiment would be similar to those used for characterizing heat transfer from different modes of boiling (see Zemansky and Dittman, 1997). The vessel containing the test fluid is submerged in a cooling water bath with sufficiently slow flowrate that the sensible heat flux from the vessel can be computed from the temperature change from outlet to inlet. If the cooling rate is sufficiently slow, the transient heat flux profile allows the fitting of a Nusselt number characterising the heat transfer coefficient. Varying the microbubble phase fraction and size distribution could be controlled by the injection time for microbubbles. Desai et al. (2018) show that fluidic oscillation generated microbubbles can achieve an average bubble size from 7 to 25 μm by varying air injection flow rate and oscillation frequency using microporous diffusers with average pore size of 2 μm in water. Changing the microporous ceramic material to larger pores can achieve large pore size. Acoustic bubble spectrometry (ABS) infers not only the bubble size distribution, but also the bubble phase fraction(Chahine and Gumerov, 2000). Changing the expo-
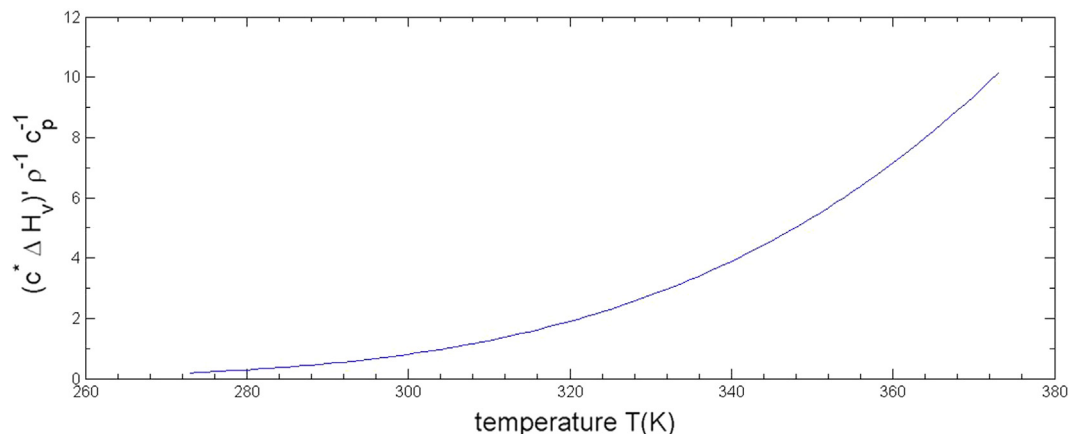
Fig. 3. The dimensionless function N_{Mpemba} / ϕ which shows the gross effect of the additional convection of the excess enthalpy by the microbubble phase. For T = 273 K, $N_{Mpemba} / \phi \sim 0.2$, but for T = 373 K, $N_{Mpemba} / \phi \sim 10$. Thus, we expect the cooling curves from this estimate to drop more rapidly at high temperatures than as they approach freezing. Of course, when the temperature reaches uniform, there is no additional convection (nor conventional buoyant convection).

sure time should influence both. ABS could gauge the phase fraction of microbubbles seeded in this way.

Unfortunately, ABS is not widely available. The ABS used for Desai et al. (2018, 2019) no longer functions due to accidental damage. Hence, validation of the theory can only proceed from explaining experiments conducted in the literature that have nearly all the prerequisites of our idealized and constructive hypothetical experimental apparatus. For such a scenario, the product of heat transfer coefficient *h* and cooling surface area *A* should be inferable, from fitting the transient heat balance (Newton's law of cooling) in a series of experiments where the microbubble phase fraction is systematically varied. Zimmerman et al. (2013) modelled heat transfer by clouds of microbubbles using Newton's law of cooling:

$$mc_p \frac{dT_l}{dt} = hA(T_{ref} - T_l) \qquad (7)$$

where T_{ref} was the gas phase temperature and hA is the product of the heat transfer coefficient and the total interfacial contact area. *m* is the mass of the liquid phase. Newton's law of cooling allows a heat balance that equates the accumulation rate of heat in the liquid on the RHS with the heat flux across the interfacial contact area. Heat transfer coefficients are usually estimated empirically for different configurations. Zimmerman et al. (2013) estimated the single microbubble heat transfer coefficient in laminar flow from dimensional analysis, and then showed that the bubble cloud heat transfer coefficient inferred from experimental data by analysis with equation (7) is the same order of magnitude.

Once the method of analysis is specified applying (7) to transient liquid temperature measurements with varying levels of microbubble phase fraction, it is necessary to find candidate experimental studies exhibiting these features. The candidate proposed here is a set of experiments performed by Mpemba and Osborne (1969) on monitoring the solidification dynamics of hot boiled water in freezers. Those authors illustrated that hot boiled tap water solidified faster than cold boiled tap water, but presented no analysis nor explanation for the phenomena observed, which is counterintuitive. Burridge and Linden (2016) debunked a generation of studies which claim that hot *pure* water cools more rapidly than cold *pure* water. Purity means the water is deionised, distilled, and degassed with no contaminants. The inescapable conclusion is how vigorous the boiling of water is by Mpemba and Osborne (1969) is the single greatest systematic difference with the carefully controlled conditions for cooling pure water reported by Burridge and Linden (2016). Mpemba and Osborne (1969) could

be viewed as incorporating uncontrolled, systematic error relative to the more recent study. However, the effects found by Mpemba and Osborne, and reproduced by countless other studies subsequently, have defied scientific explanation to date. Burridge and Linden have demonstrated that the more rapid freezing is not due to intrinsic properties of water alone, which would breach fundamental thermodynamic laws.

Intrinsic to our analysis of the experimental datasets of Mpemba and Osborne is to identify the source of the microbubbles. It is not obvious visually that there are any bubbles present in boiled tap water once it has equilibrated post-boiling. Conventionally, microbubbles generated by the saturation-nucleation mechanism have been used for industrial separations via the dissolved air flotation process (DAF). DAF (Edzwald, 1995), generates turbulent flow and intensive mixing, with a disperse population of microbubbles having a large population below 50µ size at high phase fraction (typically $\phi > 0.12$), so that the bubble cloud appears milky white due to light diffraction by the smallest microbubbles acting as light scatters. From common observation, boiled water, once settled, is transparent and colorless.

Fig. 4 is a schematic that summarizes the experimental protocols adopted by Mpemba and Osborne (1969). The most notable differences between this work and Burridge and Linden (2016) are that the tap water is vigorously boiled, and to a lesser extent that it is tap water. Tap water is of significantly variable quality with regards to trace mineral impurities. As an aside, Rehman et al. (2014) inferred mass transfer coefficients from microbubbles injected into a vessel via fluidic oscillation through a microporous diffuser. They re-used the same water for all trials, degassing and stripping the dissolved oxygen with nitrogen microbubble sparging. The rationale for this water re-use is to ensure the same composition of trace impurities in the tap water. Anecdotally, when the local water company switches reservoirs as the source, between what could grossly be described as "soft" water and "hard" water due to the mineral content, the mass transfer coefficients of the control experiment (fine bubbles produced without fluidic oscillation) jumped dramatically higher, of the order of the difference in mass transfer coefficients observed in the range of control parameter variations. In the presence of surfactants (Ribeiro and Lage, 2004) or salinity (Ribeiro and Lage, 2005), bubbles become noncoalescent. Francis and Pashley (2009) have exploited this feature for a fine bubble evaporation-based desalination process.

The origin of the bubbles is an important issue. Microbubbles are generated in a number of ways, but one of the most common is by entrainment as gas and liquid overturn. The Venturi nozzle
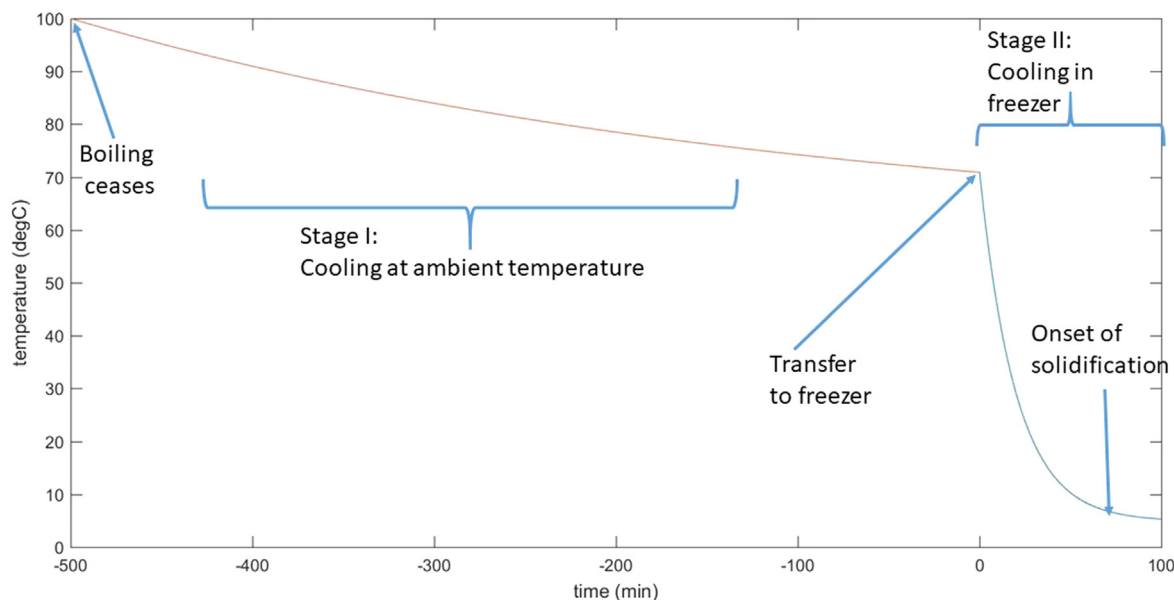
Fig. 4. A temperature profile characterising the set of experiments conducted by Mpemba and Osborne depicting the transformations undergone by the boiled tap water. The study does not specify how long the tap water is boiled for. But all specimen are treated identically according to the report by boiling. Once boiling ceases, the water is cooled by removal from the heat source, exposed to the ambient air. Once it has cooled to the desired temperature, it is poured into the freezer container and transferred to the freezer. It is observed until the onset of solidification is noted, and the time from placement into the freezer is recorded. With one such experiment, temperature histories were recorded at a point near the bottom of the container as well as one near the top.

provides a typical mechanism for entraining gas within a liquid stream (Lee et al., 2019). The combination of turbulence at the edges of the injected jet and cavitation induced by high speed liquid motion also produces microbubbles. Hann et al. (2018) shows that strong shearing of a air–liquid interface entrains small bubbles. In nature, the wind-wave action on bodies of water engenders the sea surface microlayer, populated by microbubbles due to the constant entrainment of air by the surface layer (Grammatika and Zimmerman, 2001). When boiling a liquid, not only is vapour generated in the upwelling columns, but the agitation of the interface of the bulk phases results in the entrainment of gas into the liquid and formation of small bubbles, in addition to cavitation bubbles caused by supersaturation (Zemansky and Dittman, 1997). Esmailizadeh and Mesler (1986) postulated that in nucleate boiling, ejected droplets are entrained by vapour release. When the droplets splash upon returning to the liquid surface, they entrain small bubbles. Those authors showed visualizations of the entrained bubbles. There is recent interest in the formation of vapour bubbles in film boiling on wicking meshes used to enhance film boiling heat transfer, which intensify heterogeneous vapour bubble nucleation. Such bubbles collect dissolved oxygen and persist dispersed in the liquid (Wen et al. 2018). When a boiled liquid is taken off the boil, the microbubbles persist, as the larger bubbles rise to the top surface and burst. Al-Mashhadani et al. (2012) observed that for sub 200 μm size bubbles in a buoyant convection flow, the currents in the flow are stronger than the buoyant force, hence they remain entrained. This was validated by numerical simulations using Tsuji's two fluid method as implemented in Al-Mashhadani et al (2015) with variation of the monodisperse bubble size injected into a gas-lift reactor from a fluidic oscillator. Fig. 5 shows a schematic of how boiling and stage I of the experimental protocol lead to our hypothesis about the phase fraction of microbubbles present at the start of Stage II.

There is another source of microbubble generation in heated water that also applies to boiling water – supersaturation. There are two facts which support the origin of micro/nanobubbles in heated water. First, in all but the purest water, nanobubbles are observed to be ubiquitous (Zimmerman et al. 2011b). Second, raising the temperature of a liquid generally decreases the solubility of gases. However, a liquid can be supersaturated without degassing to an appreciable extent. Mixing induced by buoyant convection within the vessel leads to the desolubilising gas solute from the liquid into the already existing nanobubbles, growing their size, and nucleating more micro/nanobubbles. Probes for dissolved oxygen do not turn up the gas held up in the bubble phase, and dilute microbubbles smaller than 100 μm are difficult to visualize by eye without high magnification.

In this paper, the hypothesis and analysis of dissolved oxygen is discussed because it is easier to measure (dissolved oxygen probes are common and relatively cheap) than dissolved nitrogen, and it has typically twice the Henry's law coefficient of nitrogen. Of course the functional form of Henry's law is identical for all dissolved, dilute gases. So in the case of dissolving air, focussing on oxygen is reasonable as it is the more mobile of the two gases.

If the source of tap water is ducted through municipal water mains, then there is ample opportunity for equilibrating with air due to long contact times. Karbowiak et al. (2010) in their Table 4 show how typical winery operations aerate wine resulting in substantial additions of dissolved oxygen, so that saturation is completely possible for oxygen in water. A typical range of water main temperatures is 5–10 °C, so that cold water before heating or boiling is likely to have achieved solubility s^*~12 mg/L. At 100 °C, according to Henry's Law (see Fig. 6), s^*=2.24 mg/L. Our argument is that degassing by heating simply inflates nano/microbubbles already present in the impure water, according to Zimmerman et al. (2011b). Diffusion in liquids is a very slow process. Boiling seeds even more micro bubbles. See Fig. 5 for the conceptualization.

Our central hypothesis that links the theory developed here and the experiments of Mpemba and Osborne (1969) is as follows. In the description of their experiments, all the water specimens were treated identically. They were, then, presumably, boiled for the same length of time. At the point in Fig. 4 where the time history begins, the specimen are treated differentially with time. Cooling
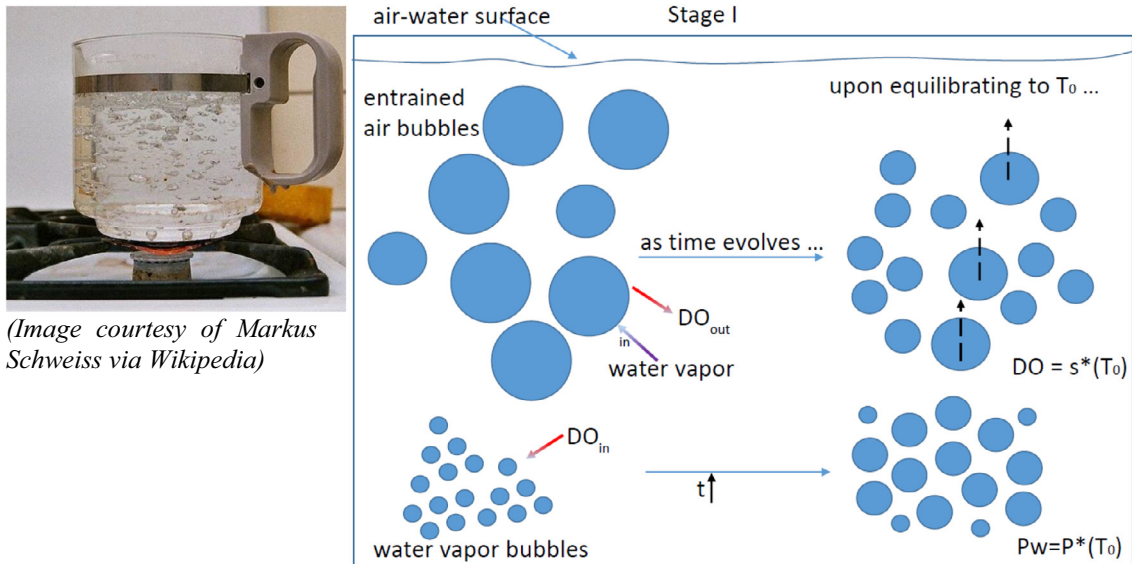
Fig. 5. (left) Natural convection boiling of water which precedes Stage I of the protocol outlined in Fig. 4. (right) Our hypothesis of oxygen transfer shown schematically. Two types of bubbles are expected to be present post-boiling – microbubbles of water vapour which will process according to natural convection currents induced by the cooler wall according to Fig. 2(right) as they are entrained by any sufficiently strong current. These microbubbles are expected to *uptake* dissolved oxygen (DO) from the water. Larger bubbles that were entrained from boiling / bubbling of the top surface have an excess of oxygen content relative to the water, so they transfer oxygen to the water by *dissolution* (DO). These oxygen transfer mechanisms will increase the size of the original microbubbles while decreasing the size of the larger coarse and fine bubbles, the largest of which will also rise to the top surface and burst. During the slow cooling of the boiled water to temperature T_0, eventually the microbubble phase equilibrates to an internal partial pressure of water vapor $P_w = P^*(T_0)$ and the concentration of dissolved oxygen reaches $s^*(T_0)$. Because of these oxygen transfers, it is our contention that the phase fraction of microbubbles ϕ depends functionally only on $s^*(T_0)$, the oxygen solubility (mg/L, typically). Given that these quantities are hypothesized to varying in opposing directions over time in Stage I according to our schematic, the functional dependence sought is a correlation between $\phi \sim 1/s^*(T_0)$. The graph considers oxygen alone as an exemplar as data on total dissolved gases in equilibrium with air is unavailable.
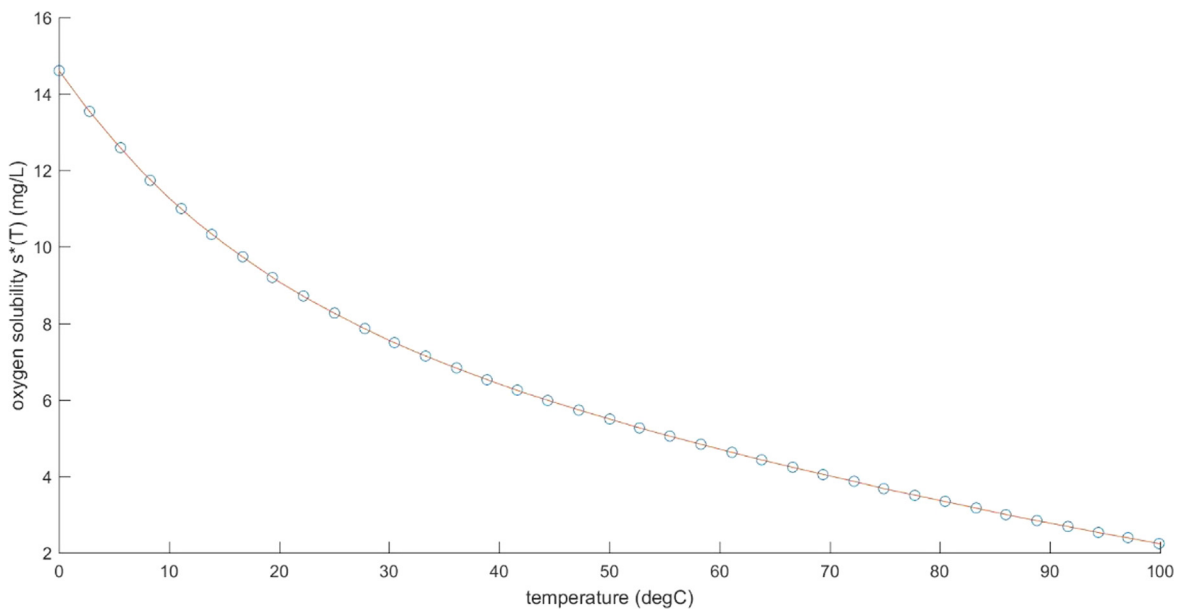
Fig. 6. Saturation solubility of oxygen in water in equilibrium with air with temperatures in the range of [0 °C,100 °C]. Computed from Henry's Law data sourced from Karbowiak et al. (2010).

in contact with ambient air is a slow process, which implies that there is sufficient contact time that the entrained microbubbles (or those present from the supersaturation of heated but not boiled tap water) trace out the solubility curve of Fig. 6 as they cool to the experimental temperature, so that the dissolved oxygen content is at the solubility curve. This volume of dissolved oxygen is nearly all transferred from the dispersed microbubble phase. Hence the

microbubble phase fraction for the initiation of the experiments for each reported initial temperature is *monotonically diminished* from the boiled value, e.g. lower initial temperatures have lower microbubble phase fractions ϕ. Our theory of microbubble mediated heat transfer predicts that the additional heat transferred due to microbubbles is proportional to the microbubble phase fraction ϕ. So a consequence of this prediction and the observation that

ϕdecreases with initial temperature for the freezing experiment is that *the rate of heat transfer observed should correlate inversely with* s∗(T).

Unfortunately, Mpemba and Osborne (1969) did not report heat transfer rates. Instead, they reported times to the onset of solidification as visually observed in the freezer. Their time data are reported in Fig. 7. As can be observed from the figure, the time to freeze famously decreases with initial temperature. Thus our task is to infer heat transfer coefficients for each experiment to test our hypothesis. Our starting point is the solution to equation (7) in this context, which is the analytic temperature profile:

$$T_l - T_{amb} = (T_0 - T_{amb})\exp(-\xi t); \text{ with } T_{amb} = 0°C \text{ and } T_l(t = t_{ref}) = T_{ref} \tag{8}$$

where $\xi = \frac{hA}{\rho c_p V_{slab}}$is the exponential rate/decay constant, which depends on the contacting surface area A of the container, the thermal load of the water within the container $\rho c_p V_{slab}$, where the density, heat capacity and volume refer to the aqueous solution. $T_0$is the initial temperature associated with each of the six experiments. Equation (8) gives the interpretation to T_{ref}as approximately the temperature where the onset of freezing occurs. This value is a key unknown for the experiments and is not reported for the six experiments that were conducted and depicted in Fig. 7. If we invert equation (8)

$$\xi = \frac{1}{t_{ref}}\ln\left(\frac{T_0}{T_{ref}}\right) \tag{9}$$

we can estimate the exponential rate/decay constant ξ, which has inverse units of time, so is clearly a rate, from the observed times to the onset of solidification, if only we knew T_{ref}.

Fortunately, Mpemba and Osborne report a seventh experiment under the same conditions which has time varying profiles for reported temperatures. Fig. 8 shows measured temperatures at two different points made over time as the container cooled in the freezer. The initial temperature does not match any of those reported in Fig. 7, but is closest to the highest temperature trialled in Fig. 7. The two positions were near the top of the container (upper curve/dataset) and near the bottom of the container (lower
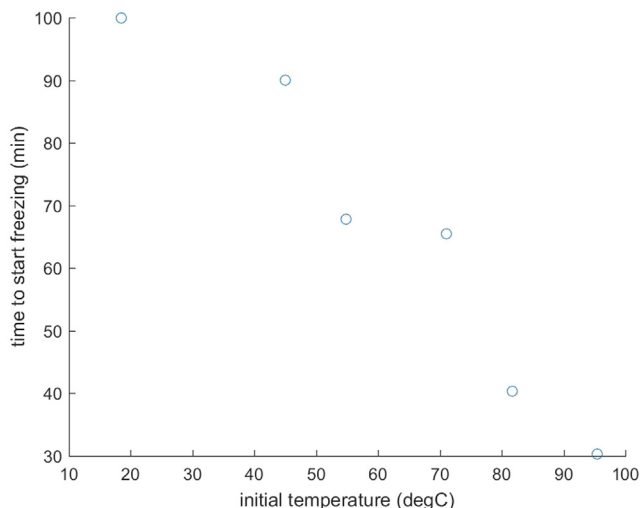

Fig. 7. Time to start freezing as reported by Mpemba and Osborne (1969) depending on the initial temperature of the protocol shown schematically in Fig. 4. Six different initial temperatures are trialled. Mpemba and Osborne (1969) do not report how long they let the boiled water sit, just what temperature it is when they place the water in the freezer. Hence, the assumption that initial temperature also implicitly defines the zero of time is made. This is consistent with Fig. 8 below – their Fig. 2.

curve / dataset). Shown are also the best fit regression curves to these temperature profiles (see Table 1).

The standard error gives some confidence – an order of magnitude for ξ and 1.6 °C for T_{ref}. We will presume that the measurement near the top of the container is the one most consistent with the initial temperatures reported in Fig. 7, hence settingT_{ref} = 4.9 °C. Of course the actual values of the estimates of ξ will depend on this value, but whether or not they correlate with s∗(T$_0$) should be immaterial to this choice, as correlation is about the functional shapes, not absolute values.

Table 2 tabulates the values of the initial temperature T_0, time for onset of freezing, the estimated rate constant ξ, and oxygen solubility at the initial temperatures∗(T$_0$), compiled and computed for the six initial temperatures of the Mpemba and Osborne (1969) experiments in Fig. 7. Fig. 9 plots the last two columns of Table 2 against each other, i.e. ξvs. 1/s∗(T$_0$). It also shows the regressed best fit line to the six data points. The linear regression curve is predicted as

$$\xi = -0.0225 + \frac{0.291}{s * (T_0)} \tag{10}$$

The astonishing feature is the excellent linear fit with a correlation for the regression of $r^2 = 0.968$. The interpretation is that 97% of the variability of the dataset in question is explained by the hypothesis that the rate of the cooling process is *linearly inversely correlated* with the solubility of oxygen equilibrated with air at the initial temperature reported for the onset of freezing time experiments. We would have been satisfied with simply computing a correlation function between the two columns of data that is inversely related, not requiring inversely linearly related. Essentially, this result signifies that during stage I, the dissolution of oxygen from the microbubbles controls the phase fraction of microbubbles present during stage II. Consequently, this phase fraction of microbubbles mediates the observed, unexpected additional heat transfer during stage II. As such, this is a strong support for our argument that each experiment seeded a microbubble phase fraction that is largely determined by the settling time to cool the boiled tap water to the initial temperature for the Mpemba and Osborne (1969) experiments. This correlation is a strong support for our theory for additional heat transfer mediated by microbubbles due to phase change dynamics near hot and cold regions, with free convective laminar flows as the mechanism.

It should be noted that equation (10) is the combination of two linear relationships that represent the theory of microbubble mediated heat transfer (11) and the ansatz that microbubble phase fraction is inversely related to s∗(T$_0$):

$$\begin{aligned}\xi &= \xi_0 + \xi_1\phi \\ \phi &= \phi_0 + \frac{\phi_1}{s*(T_0)}\end{aligned} \tag{11}$$

It probably has not escaped the reader's attention that the ξintercept in equation (10) is *negative*. Superficially, this disagrees with our theory that $\xi_1\phi$is the additional heat transfer rate due to the presence of the microbubble phase in the otherwise pure bulk liquid. There are four potential explanations for why this ξintercept having this "unexpected" sign is not pertinent:

(i) There is no pure water here. It is tap water that, according to our argument, is augmented by fully saturated dissolved oxygen at the initial temperature of the freezing experiment s∗(T$_0$). There is no baseline then for comparison of what heat transfer properties are of the microbubble-free liquid.

(ii) The range of the experiments is limited to initial temperatures in the range [18.5 °C, 95 °C]. Presumably this is because room temperature was 18.5 °C. In the original version of Fig. 7 in Mpemba and Osborne (1969), the "guide curve"
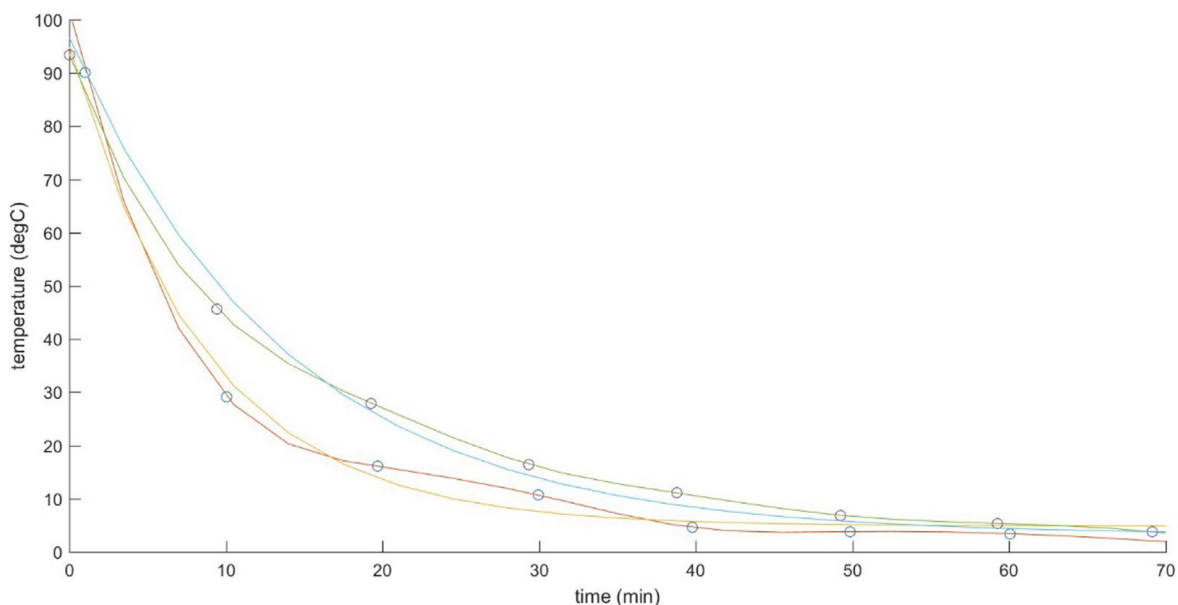
Fig. 8. Temperature history profiles for two measurement points – one near the top of the container (upper curve/data points) and one near the bottom of the container (lower curve/data points) as reported by Mpemba and Osborne (1969) for their 7th experiment following the protocol shown schematically in Fig. 4. The smooth curves are the best fit nonlinear regression curves to equation (8) for each dataset / temperature measurement position.

Table 1
$T_l = T_{ref} + (T_0 - T_{ref}) \exp(-\xi t)$ Regression Analysis for the temperature profiles of Fig. 8.

Estimated Coefficients:			Estimated Coefficients:		
	Estimate	Standard Error		Estimate	Standard Error
$\xi(\text{min}^{-1})$	0.072	0.0060	$\xi(\text{min}^{-1})$	0.12	0.013
$T_{ref}(°C)$	3.2	1.6	$T_{ref}(°C)$	4.9	1.6
$r^2 =$	0.993		$r^2 =$	0.989	

Table 2
Analysis for the time data of Fig. 7 using equation (9).

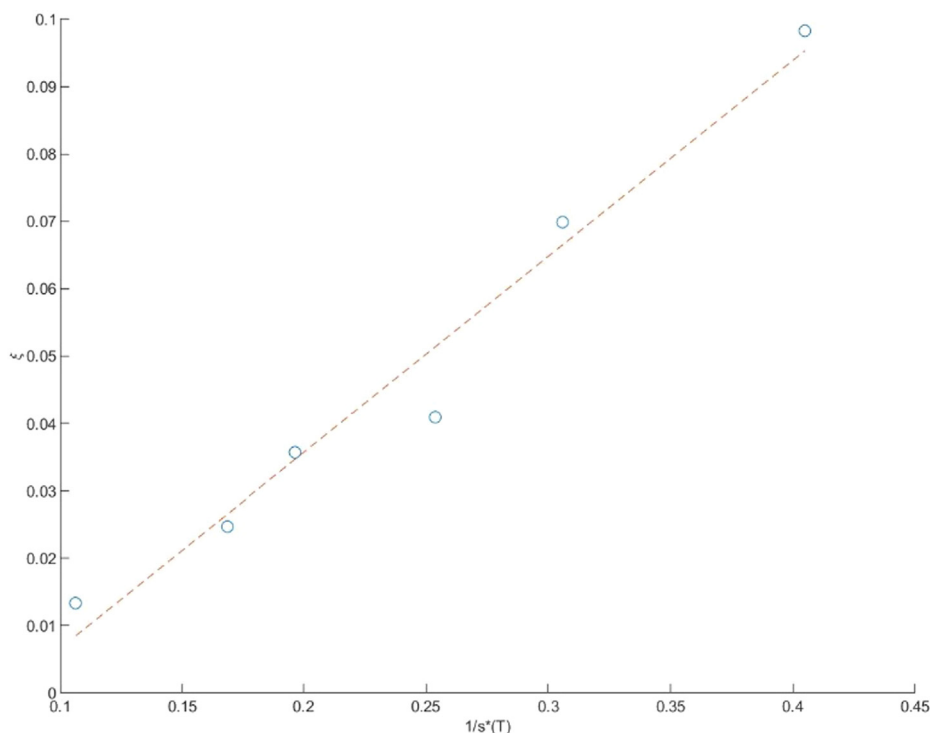| Initial temperature $T_0°C$	Time for onset of freezing (min)	Estimated rate constant ξmin^{-1}	$s*(T_0)\text{mg}/\text{L}$
18.5	100.	0.0133	9.41
45.0	90.0	0.0247	5.94
54.9	67.8	0.0357	5.09
71.0	65.4	0.0409	3.94
81.7	40.3	0.0699	3.27
95.5	30.3	0.0983	2.47

goes through the point 0 °C and 0 min for the onset of freezing. However, this point is unreachable in the experimental space because, as shown in the protocol in Fig. 4, no test water can be presented that satisfies the stage I protocol that has initial temperature between [0 °C ,18.5 °C] for stage II. If there were to be a "control liquid", it should be freshly boiled water at 100 °C. Nevertheless, the intercept lies in the "illegal range" for the experiment as is clear from Fig. 6: $1/s*(T_0)$ *never achieves a zero value.*

(iii) Many researchers argue that freshly boiled water is "degassed", i.e. has zero dissolved oxygen content, irrespective of the extrapolation of Henry's Law formula used for Fig. 6 and in the representation of $s*(T_0)$. Empirically, the Winker

method of titration is employed to determine the dissolved oxygen levels at high water temperatures (Brucker, 2021). This method demonstrates that dissolved oxygen levels diverge from Henry's Law predictions above ~ 90 °C, suggesting that the first data point of correlation uses an errant approximation of $s*(T_0 = 95.5°C)$. Table 3 gives the regression report including the standard error for the intercept, which is substantially smaller than the intercept magnitude (factor of three) so there is some confidence that the intercept is a fair approximation. Yet, the standard error in the slope, multiplied by the largest value of $1/s*(T_0)$ *is comparable to the magnitude of the ξintercept.* If this value were actually substantially larger, according to the Winkler estimation method, then confidence in the negativity of the ξintercept vanishes.

(iv) The estimation of ξhas some level of arbitrariness in the setting ofT_{ref} = 4.9 °C. But if we reflect on what it means for the actual observations of the onset of freezing in Mpemba and Osborne (1969), we have to recognize that microbubbles are now acknowledged as excellent nucleation sites for heterogeneous crystallization. Kuang et al. (2019) have characterized morphological control of gas hydrates crystallized from microbubble seeding. Fatemi et al. (2019) report a faster rate of crystallization of paracetamol in microfluidic channels when seeded with microbubbles. If our ansatz is correct that microbubbles are present in the six trials of Mpemba and Osborne (1969) at substantially different levels, the first ice crystals formed visually are likely to have occurred at the highest measured liquid temperature with the highest volume fraction of microbubbles (largest initial temperature), with the opposite expected for the lowest volume microbubble volume fraction (lowest initial temperature). This plausibly would make some difference in the inferred heat transfer coefficients ξ, thereby influencing the estimate of the ξintercept. It is an experiment for freezing onset, but our interest lies in cooling rates.

Ideally, a theory should be tested for the quantitative predictions that are consequences under carefully controlled

Fig. 9. Plot of ξ vs. $1/s*(T_0)$ using the tabulated values in Table 2 for the six experiments of Mpemba and Osborne that report time to the onset of freezing for specimens of hot water at various initial temperatures. The circles are the data points, and the dashed line is the best fit linear regression. The ξ intercept (units of s^{-1}) is estimated as -0.0225; the slope is estimated as 0.291 mg L^{-1} s^{-1}, with correlation coefficient $r^2 = 0.968$. $s*$ refers to the solubility of oxygen in mg/L.

Table 3
Regression Analysis for Fig. 9, $\xi = -0.0225 + \frac{0.291}{s*(T_0)}$.

Estimated Coefficients:	Estimate	Standard Error
Intercept (s^{-1})	-0.0225	0.00680
Slope (mg L^{-1} s^{-1})	0.291	0.0263

circumstances so that the predicted changes can be assessed against measurements. In this case, the microbubble phase fraction that is smaller than ~ 200 μm in individual bubble size should be controlled and measured, and the additional heat flux over the case of no microbubbles should be measured. Desai et al. (2019) demonstrated that the most accurate approach to infer bubble phase fraction is acoustic bubble spectrometry. Unfortunately, this is rare instrumentation, and the device used for Desai et al. (2018, 2019) is damaged and inoperable.

The next best approach to testing a new theory is to determine whether or not the theory is consistent with previously unexplained experiments already in the literature. There are no experiments in the literature explicitly testing the heat transfer capabilities of controlled microbubble dispersions. The candidate class for an unexplained set of heat transfer experiments stem from Mpemba and Osborne (1969) which describe a seemingly anomalous faster cooling rate for hot water than cold water. The concept of a Mpemba effect cooling where pure hot water cools faster than pure cold water has been debunked by recent careful experiments of Burridge and Linden (2016). The cooling rates are exactly as predicted by the physical properties -- thermal conductivity, density and heat capacity of water at the proscribed temperatures. Consequently, the inescapable conclusion is that the observed reversal of cooling rates / times to solidification in this class of experiments must be based on uncontrolled, systematic error relative to the carefully controlled experiments of Burridge and Linden (2016).

5. Conclusions

Motivated by the theory and experiments that established the time scales for the evaporation (and therefore condensation) dynamics of microbubbles in water (Zimmerman et al. 2013), it is hypothesized that microbubbles rapidly equilibrate their temperature (on the time scales of some milliseconds for microbubbles ~ 200 μm or smaller in diameter) with their local liquid environment. Microbubbles that pass a hot surface, therefore, vaporize some of their surrounding water as they thermochemically equilibrate in hot regions / near a hot wall. This means that the vapour phase of the microbubble now carries the latent heat of vaporization extracted from the hot wall. Conversely, as this "hot and humid" microbubble approaches a cold wall / cold region of liquid, it is superheated and supersaturated with water vapour relative to the surrounding water. It therefore experiences a strong thermochemical driving force to condense its supersaturated humidity, thereby releasing the latent heat of the water that condensed. If free convection, such as in the canonical hot wall-cold wall problem, transports the microbubble phase, microbubbles would then be "recycled" as carriers of the latent heat of vaporisation, thereby acting as agents for additional heat transfer. An analysis of the heat transport with this additional carrying of the latent heat of vaporization associated with the saturated bubble phase gives a *quantitative* prediction that the additional heat flux is proportional to the phase fraction of microbubbles.

Our hypothesis is that the original experiments of (Mpemba and Osborne, 1969) differ principally from those of Burridge and Linden (2016) by the supposition that the former vigorously boiled tap water boiled, while the latter boiled their purified water. It is argued that this difference is sufficiently controlled by (Mpemba and Osborne, 1969) so that heat transfer analysis can be conducted, and that the source of microbubbles from either boiling or heating (saturation-nucleation mechanism) can be characterised by the

solubility of dissolved oxygen at the initial temperature of the freezing experiments. This hypothesis is tested by demonstrating that indeed, the inferred heat transfer coefficients (HTCs) from the Mpemba and Osborne (1969) experiments with this *de novo* analysis correlates linearly with the inverse solubility at the initial solution temperature. Indeed, the HTCs inferred and tabulated in Table 2 show approximately a 7.4:1 ratio from the highest initial temperature to the smallest. Because of this strong correlation, it is concluded that the hypothesis that microbubbles are present and act as the agents for additional phase change mediated heat convection is supported. Of course this is a functional argument, based on the correlation, not a quantitative argument, suggesting that the quantitative theory is correct up to a proportionality correction factor. The experiment only tests that the additional heat flux is proportional to the phase fraction of microbubbles, not that the predicted constant of proportionality in the theory holds. This would indeed require measurement of the microbubble phase fraction.

It has been argued that a microbubble condenser, designed in the airlift loop configuration, would benefit from faster liquid-vessel heat transfer due to the proposed mechanism for additional microbubble mediated heat transfer due to phase change dynamics. The purpose of this paper is to make the case for such an investigation. The theory proposed here, and supported by consistency with the experiments of Mpemba and Osborne (1969), has the promise of widespread applicability to heat transfer applications that are limited to cheap heat transfer fluids – a microbubble dispersion in water of sufficiently small average bubble size so that the "shelf-life" exceeds the operational duty duration. Of course, once the "shelf-life" has been exceeded, injecting fresh air microbubbles with fluidic oscillation is a cheap operation.

Author contribution

The sole author is the sole authority on the work and the paper. The Acknowledgments section expresses thanks for those who encouraged, discussed or funded the work as it progressed.

Declaration of Competing Interest

The authors declare that they have no known competing financial interests or personal relationships that could have appeared to influence the work reported in this paper.

Acknowledgements

References

Abdulrazzaq, N., Al-Sabbagh, B., Rees, J.M., Zimmerman, W.B., 2015. Separation of azeotropic mixtures using air microbubbles generated by fluidic oscillation. AICHEJ. https://doi.org/10.1002/aic.15097.

Abdulrazzaq, N., Al-Sabbagh, B., Rees, J.M., Zimmerman, Zimmerman, W.B., 2016. Purification of Bioethanol Using Microbubbles Generated by Fluidic Oscillation: A Dynamical Evaporation Model. Ind. Eng. Chem. Res. 55, 12909–12918.

Al-Mashhadani, M.K.H., Bandulasena, H.C.H., Zimmerman, W.B., 2012. CO$_2$ mass transfer induced through an airlift loop by a microbubble cloud generated by fluidic oscillation. Ind. Eng. Chem. Res. 51 (4), 1864–1877.

Al-Mashhadani, M.K.H., Wilkinson, S.J., Zimmerman, W.B., 2015. Airlift bioreactor for biological applications with microbubble mediated transport processes. Chem. Eng. Sci. 137, 243–253.

Al-yaqoobi, A., Hogg, D., Zimmerman, W.B., 2016. Microbubble distillation for ethanol-water separation. Int. J. Chem. Eng. 5210865. https://doi.org/10.1155/2016/5210865.

Brucker, M.Z., 2021. The Winkler Method - Measuring Dissolved Oxygen, Montana State University, https://serc.carleton.edu/microbelife/research_methods/environ_sampling/oxygen.html.

Burridge, H.C., Linden, P.F., 2016. Questioning the Mpemba effect: hot water does not cool more quickly than cold. Sci. Rep. 6, 37665.

Chahine, G.L., Gumerov, N.A., 2000. An inverse method for the acoustic detection, localization and determination of the shape evolution of a bubble. Inverse Probl. 16, 1–20.

Desai, P.D., Hines, M.J., Riaz Zimmerman, W.B., 2018. Resonant pulsing frequency effect for much smaller bubble formation with fluidic oscillation. Energies 11, 2680. https://doi.org/10.3390/en11102680.

Desai, P., Ng, W., Hines, M., Riaz, Y., Tesar, V., Zimmerman, W., 2019. Comparison of bubble size distributions inferred from acoustic, optical visualisation, and laser diffraction. Colloids Interfaces 3 (4), 65.

Desai, P.D., 2017. PhD thesis, University of Sheffield.

Edzwald, JK, 1995. Principles and applications of dissolved air flotation. Water Science and Technology 31, 1–23.

Esmailizadeh, L., Mesler, R., 1986. Bubble entrainment with drops. J. Colloid Interface Sci. 110 (2), 561–574.

Fatemi, N., Dong, Z., Van Gerven, T., Kuhn, S. Microbubbles as heterogeneous nucleation sites for crystallization in continuous microfluidic devices. Langmuir 35(1), 60–69.

Francis, M.J., Pashley, R.M., 2009. Thermal desalination using a non-boiling bubble column. Desalin. Water Treat. 12, 155–161.

Grammatika, M., Zimmerman, W.B., 2001. Microhydrodynamics of flotation processes in the sea surface layer. Dynam. Oceans Atmospheres 34, 327–348.

Hann, D.B., Cherdantsev, A.V., Azzopardi, B.J., 2018. Study of bubbles entrapped into a gas-sheared liquid film. Int. J. Multiph. Flow 108, 181–201.

Karbowiak, T., Gougeon, R.D., Alinc, J.-B., Brachais, L., Debeaufort, F., Voilley, A.E., Chassagne, D., 2010. Wine Oxidation and the Role of Cork. Crit. Rev. Food Sci. Nutr. 50, 20–52.

Kuang, Y., Feng, Y., Yang, L., Song, Y., Zhao, J., 2019. Effects of micro-bubbles on the nucleation and morphology of gas hydrate crystals. Phys. Chem. Chem. Phys. 21, 23401–23407.

Kumar, V., Faizee, B., Mridha, M., Nigam, K.D.P. Numerical studies of a tube-in-tube helically coiled heat exchanger. Chem. Eng. Process. 47(12), 2287–2295.

Lee, C.H., Choi, H., Jerng, D.-W., Kim, D.E., Wongwises, S., Ahn, H.S., 2019. Experimental investigation of microbubble generation in the venture nozzle. Int. J. Heat Mass Transf. 136, 1127–1138.

Lervik, A., Bresme, F., Kjelstrup, S., 2009. Heat transfer in soft nanoscale interfaces: The influence of interface curvature. Soft Matter 5, 2405.

Matheson, R., 2015. Toward cheaper water treatment. MIT News. https://news.mit.edu/2015/cheaper-fracking-water-treatment-0716, 2015.

Mpemba, E.B., Osborne, D.G., 1969. Cool?. Phys. Educ. 4, 172–175.

Ribeiro, C.P., Lage, L.P.C., 2004. Experimental study on bubble size distributions in a direct-contact evaporator. Braz. J. Chem. Eng. 21 (1), 69–81.

Ribeiro, C.P., Lage, L.P.C., 2005. Gas-liquid direct-contact evaporation: A review. Chem. Eng. Technol. 28 (10), 1081–1107.

Rehman, F., Medley, G.J., Bandulasena, H., Zimmerman, W.B. Fluidic oscillator-mediated microbubble generation to provide cost effective mass transfer and mixing efficiency to the wastewater treatment plants. Environ. Res. 137, 32–39, doi:10.1016/j.envres.2014.11.017

Shaqfeh, E.S.G., 1988. A nonlocal theory for the heat transport in composites containing highly conducting fibrous inclusions. Phys. Fluids 31 (9), 2405–2425.

Wen, R., Xub, S., Leeb, Y.-C., Yang, R., 2018. Capillary-driven liquid film boiling heat transfer on hybrid mesh wicking Structures. Nano Energy 51, 373–382.

Wies, R., Jannsen, N., 2014. Review and Testing of Steffes Electric Thermal Storage Unit with Grid-Interactive Frequency Regulation. University of Alaska report. http://acep.uaf.edu/media/127462/Final_Report_ETS_Grid_Frequency_Test_Final_1-22-2014_415PM.pdf, 2014.

You, S.M., Kim, J.H., 2003. Effect of nanoparticles on critical heat flux of water in pool boiling heat transfer. Appl. Phys. Lett. 83, 3374.

Zalba, B., Marin, J.-M., Cabeza, L.F. Mehling, H., 2003. Review on thermal energy storage with phase change: materials, heat transfer analysis and applications. Appl. Therm. Eng. 23, 251–283.

Zemansky, M.W., Dittman, R., 1997. Heat and Thermodynamics, McGraw; 7th ed.

Zimmerman, W.B.J., 2006. Multiphysics Modelling with Finite Element Methods, World Scientific Series on Stability, Vibration and Control of Systems, Vol 18., Singapore, 2006.

Zimmerman, W.B., Rees, J.M., 2007. Rollover instability due to double diffusion in a stably stratified cylindrical tank. Phys. Fluids 19, 123604.

Zimmerman, W.B., Hewakandamby, B.N., Tesař, V., Bandulasena, H.C.H., Omotowa, O.A., 2009. On the design and simulation of an airlift loop bioreactor with microbubble generation by fluidic oscillation. Food Bioprod. Process. 87, 215–227.

Zimmerman, W.B., Zandi, M., Bandulasena, H.C.H., Tesar, V., Gilmour, D.J., Ying, K., 2011a. Design of an airlift loop bioreactor and pilot scales studies with fluidic oscillator induced microbubbles for growth of a microalgae Dunaliella salina. Appl. Energy 88, 3357–3369.

Zimmerman, W.B., Tesař, V., Bandulasena, H.C.H., 2011b. Towards energy efficient nanobubble generation with fluidic oscillation. Curr. Opin. Colloid Interface Sci. 16 (4), 350–356.

Zimmerman, W.B., Al-Mashhadani, M.K.H., Bandulasena, H.C.H., 2013. Evaporation dynamics of microbubbles. Chem. Eng. Sci. 101, 865–877.